

Acoustic radiation-based optimization of the placement of actuators for active control of noise transmitted through plates

Stanislaw Wrona^a, Marek Pawelczyk^a, Jordan Cheer^b

^a*Silesian University of Technology, Department of Measurements and Control Systems, Gliwice, Poland*

^b*Institute of Sound and Vibration Research, University of Southampton, Southampton, United Kingdom*

Abstract

Active Structural Acoustic Control (ASAC) is mostly performed using a passive noise barrier, vibration actuators, sensors and a control system. ASAC reduces or alters the vibration of the barrier structure in a way that blocks the noise propagation through it. However, it is crucial that the actuators are appropriately arranged to be able to effectively control the vibration of the barrier. If the actuators were not optimally arranged, then certain modes of the structure may be uncontrollable, or require a very high control effort. Hence, the locations of the actuators should be determined by a careful optimization process employing a model of the structure. A common approach is to maximize the controllability of the system over a defined frequency range of operation. However, such an optimisation procedure often results in a solution that considers numerous vibration modes, only some of which are acoustically-relevant. That is, certain structural modes may vibrate considerably, but their contribution to the noise transmission and radiation would be negligible. Therefore, in the presented research a new acoustic radiation-based approach to the optimisation of the arrangement of actuators is proposed. A model of acoustic radiation is introduced and new cost functions are formulated to focus on modes that strongly contribute to noise transmission or radiation by the noise barrier. For the considered system, this enables an increase in the controllability measure of more than 5 dB for acoustically-relevant modes, which is similar to the level of improvement achieved when the number of actuators is doubled.

Keywords: Noise control, Noise reduction, Mathematical modelling, Optimization process, Actuators arrangement, Acoustic radiation

1. Introduction

Exposure to excessive acoustic noise is an important problem in modern society and it thus stimulates the development of a variety of noise reduction techniques. One such approach is to separate the recipients from the noise source using noise barriers. However, common passive barriers are often ineffective for low-frequency noise. They also tend to be thick, heavy, and introduce considerable heat insulation that may cause additional problems in certain applications. To overcome this limitation, passive barriers can be complemented with or replaced by

Email addresses: stanislaw.wrona@polsl.pl (Stanislaw Wrona), marek.pawelczyk@polsl.pl (Marek Pawelczyk), j.cheer@soton.ac.uk (Jordan Cheer)

Preprint submitted to Elsevier

March 30, 2020

actively controlled barriers, which incorporate control sources that may be either acoustic, such as loudspeakers, or structural, such as vibration actuators [1][2][3][4]. These active systems are most effective in the low-frequency range, where passive insulation fails. Under certain circumstances, even openings with dedicated active noise control systems can be integrated into barriers to allow air flow [5][6][7].

Active noise barriers present many advantages over their passive counterparts, but they have to be carefully implemented in order to operate efficiently and achieve a high level of performance. One of the critical aspects in the design of an active barrier is the arrangement of the actuators, such that they are able to effectively control the vibration of the plate that forms the noise barrier. It is noteworthy that the optimization of the actuator arrangement is also an important step in the design of systems where plates are intentionally designed to emit sound [8].

Different techniques have been proposed over the years to optimize the arrangement of actuators for control applications. One approach primarily focuses on selecting a control strategy and defining a performance index, and then simultaneously optimizing the locations of the actuators and the controller parameters. Liu et al. [9] used a genetic algorithm and the spatial H_2 norm of the closed-loop system as the performance index. Arabyan and Chemishkian [10] presented a computational method to design an H_∞ controller and the corresponding optimal actuator locations. Kumar et al. [11] considered the performance of an LQR controller as an objective. Chhabra et al. [12] used the modified control matrix and the singular value decomposition approach for optimal placement of piezoelectric actuators. However, in such approaches, optimality of the obtained solution is dependent on the choice of the control strategy.

Another approach concentrates on an open-loop system analysis, which is independent of the controller choice. The controllability Gramian was used in the optimization criterion by Leleu et al. [13]. Hale and Daraji [14] presented a modified H_∞ norm based method for the optimal placement of piezoelectric sensor/actuator pairs mounted on a cantilever plate. The optimal placement of piezoelectric actuators for active vibration control of a membrane structure using the controllability Gramian and the particle swarm optimization algorithm was studied by Liu et al. [15].

The aforementioned studies provide methods for the optimization of actuator locations mainly for the Active Vibration Control (AVC) of plates. Although the same actuator configuration can also be used for Active Structural Acoustic Control (ASAC) as employed in active noise barriers [16][17][18][19][20], it is not necessarily the optimum arrangement for this purpose. The optimization of the actuator arrangement for vibration control entails a search for a solution that generally reaches a trade-off between controlling numerous modes of vibration. Some of these structural modes may radiate sound efficiently, whilst others may vibrate considerably without contributing strongly to the noise transmission or radiation; as a result, these modes do not need to be controlled in the context of a noise barrier. Therefore, in the presented research, a new acoustic radiation-based approach to the optimization of the arrangement of actuators on a plate for the control of noise transmission is proposed. A model of acoustic radiation is introduced into the optimization process and new cost functions are formulated to focus on modes that are truly relevant to the overarching goal of the barrier, which is to block the transmission of noise. The main contribution of this paper is thus providing new insight into the optimization process that should be adopted for the positioning of actuators in active noise barriers.

This paper is organized as follows. Section 2 presents a model of the vibroacoustic system, including both vibration and acoustic radiation phenomena. Section 3 is devoted to the verification of the developed model utilizing a real experimental setup. Then, Section 4 introduces the proposed actuator arrangement optimization process, including formulation of the optimization

problem, introduction of new acoustic radiation-based cost functions and a brief description of the employed memetic algorithm. Then, in Section 5 the obtained optimization results are presented and analysed. Finally, advantages and limitations of the proposed approach are pointed out and discussed, and conclusions for future research are drawn.

2. Model of the vibroacoustic system

In this Section, a model of the vibroacoustic system is presented. The derivation begins with a description of the free vibrations of an orthotropic rectangular plate with inertial actuators attached to its surface. The Kirchhoff-Love theory of thin plates is used for this purpose. The boundary conditions of the plate are assumed to be fully-clamped. Then, the Rayleigh-Ritz method is employed to define an approximate solution, which provides the natural frequencies and mode shapes of the vibrating system. Subsequently, an appropriate Green's function is used to estimate the acoustic radiation from the obtained modes. Finally, a state space form of the model is developed, which facilitates the controllability analysis and formulation of the cost functions used in the optimization of the actuator locations.

Model of plate vibration

For an orthotropic and homogeneous plate, which occupies the $x-y$ plane in the reference stress-free state, free vibrations are governed by a differential system [21]

$$D_x \frac{\partial^4 w}{\partial x^4} + 2(D_x \nu_y + 2D_{xy}) \frac{\partial^4 w}{\partial x^2 \partial y^2} + D_y \frac{\partial^4 w}{\partial y^4} + \rho_p h \frac{\partial^2 w}{\partial t^2} = 0, \quad (1)$$

for

$$x \in (0, a), \quad y \in (0, b), \quad t > t_0 > 0, \quad (2)$$

where

$$D_x = \frac{E_x h^3}{12(1 - \nu_x \nu_y)}, \quad D_y = \frac{E_y h^3}{12(1 - \nu_x \nu_y)}, \quad D_{xy} = \frac{G h^3}{12}. \quad (3)$$

The initial conditions are defined by

$$w(x, y, t_0) = 0, \quad \left. \frac{\partial w(x, y, t)}{\partial t} \right|_{t=t_0} = 0. \quad (4)$$

In Eq. (1)-(4) the function $w(x, y, t)$ denotes the displacement of the plate from the reference state in the z -direction at time $t > 0$ and position (x, y) ; the lengths of the edges of the rectangular plate are assumed to be equal to a and b , respectively; D_x , D_y , and D_{xy} are orthotropic rigidities of the plate; E_x and E_y are the Young's moduli along the x and y directions, respectively; G is the shear modulus; ν_x and ν_y are the Poisson ratios corresponding to the x and y directions, respectively; ρ_p is the mass density of the plate material; and h is the plate thickness.

Considering only the transverse motion and neglecting the effect of rotary inertia, the kinetic and strain energies of the plate, T_p and U_p , can be written as

$$T_p = \frac{\rho_p h}{2} \iint_{S_p} \left(\frac{\partial w}{\partial t} \right)^2 dx dy, \quad (5a)$$

$$U_p = \frac{1}{2} \iint_{S_p} \left\{ D_x \left(\frac{\partial^2 w}{\partial x^2} \right)^2 + D_y \left(\frac{\partial^2 w}{\partial y^2} \right)^2 + 2D_x \nu_y \frac{\partial^2 w}{\partial x^2} \frac{\partial^2 w}{\partial y^2} + 4D_{xy} \left(\frac{\partial^2 w}{\partial x \partial y} \right)^2 \right\} dx dy, \quad (5b)$$

where S_p is the surface area of the plate. The definition of the kinetic and strain energies of the plate is particularly important, as the Rayleigh-Ritz method is used in this research to find an approximate solution of the differential system (the method is based on the definition of an energy functional).

Inclusion of the actuators

The plate considered in this paper is assumed to be employed as an actively controlled acoustic barrier. For this purpose, inertial actuators are bonded to the surface of the plate. Their mass is often comparable to the mass of the plate and, therefore, they have a considerable impact on the dynamic response of the plate (both natural frequencies and mode shapes). Hence, in order to develop a model of the system that would remain valid after mounting the actuators, they must also be included in the mathematical modelling.

The actuators can be considered to be small in size compared to the dimensions of the plate, hence, their impact (loading of the plate) can be represented by additional concentrated masses. The influence of the strain caused by these elements bonded to the plate surface is neglected. Assuming also a perfect bonding and neglecting the stiffness of the actuators, the total energy introduced into the system by the actuators can be represented by the kinetic energy expressed as

$$T_a = \sum_{i=1}^{N_a} \frac{1}{2} \left\{ m_{a,i} \left(\frac{\partial w}{\partial t} \right)^2 \right\} \Big|_{x=x_{a,i}, y=y_{a,i}}, \quad (6)$$

where N_a is the number of actuators bonded to the surface of the plate; $m_{a,i}$ is the mass of the i -th actuator; and $x_{a,i}$ and $y_{a,i}$ are the coordinates of the i -th actuator, respectively. For the sake of brevity, mathematical modelling of actuators bonded to the plate is presented separately from the differential system of the vibrating plate, defining only the kinetic energy related to the actuators (as it is most important for the Rayleigh-Ritz method used to solve the resulting differential system).

The Rayleigh-Ritz method

The Rayleigh-Ritz method is used to calculate an approximate solution of the presented differential system, obtaining its natural frequencies and mode shapes. To utilize this method, the total energy of the system (derived in the previous part of this section) and carefully selected trial functions need to be defined. More detailed information regarding the Rayleigh-Ritz method itself is provided in [22].

For free vibration of the plate, the solution of w can be expressed in the required form using a predetermined set of admissible trial functions

$$w(x, y, t) = \sum_{i=1}^N \phi_i(x, y) q_i(t) = \boldsymbol{\phi}^T \mathbf{q}, \quad (7)$$

where \mathbf{q} is a generalized plate displacement vector; $\boldsymbol{\phi}$ is a vector, which represents a set of time-invariant trial functions $\phi_i(x, y)$ —in this paper, characteristic orthogonal polynomials having the property of Timoshenko beam functions are used; and the superscript T denotes the transpose operator. All of the mentioned vectors are of dimension $(N \times 1)$, where N is the number of employed trial functions. The procedure for forming orthogonal polynomial trial functions for rectangular plates is described in detail in [23].

Total energy definition

Utilizing Eq. (7), the total kinetic and potential energies, T and U , defined by Eqs. (5) and (6), can also be written as functions of the generalized plate displacement vector \mathbf{q} , mass matrix \mathbf{M} of dimensions $(N \times N)$ and stiffness matrix \mathbf{K} of dimensions $(N \times N)$ as [24]

$$T = T_p + T_a = \frac{1}{2} \dot{\mathbf{q}}^T \mathbf{M} \dot{\mathbf{q}}, \quad U = U_p = \frac{1}{2} \mathbf{q}^T \mathbf{K} \mathbf{q}. \quad (8)$$

The overall mass matrix \mathbf{M} is calculated as the sum of matrices related to different energy components

$$\mathbf{M} = \mathbf{M}_p + \mathbf{M}_a, \quad (9)$$

where \mathbf{M}_p and \mathbf{M}_a correspond to the kinetic energies of the plate and the actuators, respectively. The elements of the mass matrices introduced in Eq. (9) are defined as:

$$M_{p,ij} = \rho_p h \iint_{S_p} \phi_i \phi_j dx dy, \quad (10a)$$

$$M_{a,ij} = \sum_{k=1}^{N_a} \left\{ m_{a,k} \phi_i \phi_j \right\} \Big|_{\substack{x=x_{a,k} \\ y=y_{a,k}}}. \quad (10b)$$

The elements K_{ij} of the stiffness matrix \mathbf{K} can be derived as

$$K_{ij} = \iint_{S_p} \left\{ D_x \frac{\partial^2 \phi_i}{\partial x^2} \frac{\partial^2 \phi_j}{\partial x^2} + D_y \frac{\partial^2 \phi_i}{\partial y^2} \frac{\partial^2 \phi_j}{\partial y^2} + 2D_{xy} \frac{\partial^2 \phi_i}{\partial x^2} \frac{\partial^2 \phi_j}{\partial y^2} + 4D_{xy} \frac{\partial^2 \phi_i}{\partial x \partial y} \frac{\partial^2 \phi_j}{\partial x \partial y} \right\} dx dy. \quad (11)$$

Equation of the vibrating structure and a harmonic solution

Using the Lagrange equation of the second kind, the equation of a vibrating structure can be obtained using the stiffness and mass matrices defined above as

$$\mathbf{M} \ddot{\mathbf{q}} + \mathbf{K} \mathbf{q} = \mathbf{Q}, \quad (12)$$

where \mathbf{Q} is the vector of generalized forces of dimensions $(N \times 1)$. In this paper, inertial actuators are considered and for the purpose of their positioning, their action can be simplified and taken into account as a force acting at a point. Therefore, the control vector \mathbf{u} of dimensions $(N_a \times 1)$ can be defined as

$$\mathbf{u} = [f_1, f_2, \dots, f_{N_a}]^T, \quad (13)$$

where f_i is a force generated by the i -th actuator. Then, the vector of generalized forces can be expressed as

$$\mathbf{Q} = \left[\phi \Big|_{\substack{x=x_{a,1} \\ y=y_{a,1}}}, \phi \Big|_{\substack{x=x_{a,2} \\ y=y_{a,2}}}, \dots, \phi \Big|_{\substack{x=x_{a,N_a} \\ y=y_{a,N_a}}} \right] \mathbf{u}. \quad (14)$$

The harmonic solution of Eq. (12) gives the eigenvector matrix Φ of dimensions $(N \times N)$ and N eigenfrequencies ω_i . Replacing \mathbf{q}^T by $\Phi \mathbf{v}$, and multiplying Eq. (12) on the left by Φ^T gives

$$\Phi^T \mathbf{M} \Phi \ddot{\mathbf{v}} + \Phi^T \mathbf{K} \Phi \mathbf{v} = \Phi^T \mathbf{Q}, \quad (15)$$

where \mathbf{v} denotes a modal displacement vector of dimensions $(N \times 1)$:

$$\mathbf{v} = [v_1, v_2, \dots, v_N]^T. \quad (16)$$

Taking advantage of the orthonormality of the eigenvectors in the matrix Φ , the modal mass matrix becomes a unit matrix \mathbf{I}_N of dimensions $(N \times N)$ and the corresponding modal stiffness matrix becomes a diagonal matrix Ω of N eigenvalues ω_i^2 [25], which gives

$$\Phi^T \mathbf{M} \Phi = \mathbf{I}_N, \quad (17a)$$

$$\Phi^T \mathbf{K} \Phi = \Omega = [\text{diag}(\omega_1^2, \omega_2^2, \dots, \omega_N^2)]. \quad (17b)$$

Then, by substituting Eq. (17) into Eq. (15), gives

$$\ddot{\mathbf{v}} + \Omega \mathbf{v} = \Phi^T \mathbf{Q}. \quad (18)$$

To provide a better representation of the behaviour of a real system, this is extended to

$$\ddot{\mathbf{v}} + \Xi \dot{\mathbf{v}} + \Omega \mathbf{v} = \Phi^T \mathbf{Q}, \quad (19)$$

where $\Xi \dot{\mathbf{v}}$ is a term introduced to include the damping in the system, and Ξ is a diagonal matrix of dimensions $(N \times N)$ defined as:

$$\Xi = [\text{diag}(2\xi_{d,1}\omega_1, 2\xi_{d,2}\omega_2, \dots, 2\xi_{d,N}\omega_N)]. \quad (20)$$

In Eq. (20), the damping ratios, $0 < \xi_{d,i} < 1$, are calculated using the thermoelastic damping model for elastic plates described in detail in [26]. The damping mechanism could also be included at the beginning of the modelling in the form of complex bending rigidities. However, this would substantially complicate the derivation. Introducing it instead at this point preserves the brevity of the derivation and leads to an equivalent solution. This approach was also used, e.g., in [13].

State space model

To allow standard control analysis tools to be utilised, Eq. (19) can be written in the usual state-space form

$$\dot{\mathbf{x}} = \mathbf{A}\mathbf{x} + \mathbf{B}\mathbf{u} \quad (21)$$

with the state vector \mathbf{x} of dimensions $(2N \times 1)$ given by

$$\mathbf{x} = [\dot{v}_1, \omega_1 v_1, \dot{v}_2, \omega_2 v_2, \dots, \dot{v}_N, \omega_N v_N]^T. \quad (22)$$

The state matrix $\mathbf{A} = [\text{diag}(\mathbf{A}_1, \mathbf{A}_2, \dots, \mathbf{A}_N)]$ with dimensions $(2N \times 2N)$, is defined by

$$\mathbf{A}_i = \begin{bmatrix} -2\xi_{d,i}\omega_i & -\omega_i \\ \omega_i & 0 \end{bmatrix}, \quad i = 1, 2, \dots, N. \quad (23)$$

The matrix \mathbf{B} , of dimensions $(2N \times N_a)$, can be expressed as

$$\mathbf{B} = [\text{diag}(\mathbf{b}_1, \mathbf{b}_2, \dots, \mathbf{b}_{3N})] \Phi^T \begin{bmatrix} \phi \Big|_{\substack{x=x_{a,1} \\ y=y_{a,1}}} \\ \phi \Big|_{\substack{x=x_{a,2} \\ y=y_{a,2}}} \\ \dots \\ \phi \Big|_{\substack{x=x_{a,N_a} \\ y=y_{a,N_a}}} \end{bmatrix}, \quad (24)$$

where $\mathbf{b}_i = [1 \ 0]^T$.

Acoustic radiation

The aim of this derivation is to determine an estimate of the radiated acoustic power corresponding to the i -th vibration mode of the considered plate. To describe the acoustic radiation of the plate, it has been assumed that it is placed in an infinite rigid baffle (cf. Fig. 1). Adopting an appropriate Green's function that has been derived in [27] and [28], the modal sound pressure amplitude $p_i(x, y, z)$ can be calculated as

$$p_i(x, y, z) = \frac{k_e a b}{4\pi^2} \rho_e c \iint_{-\infty}^{+\infty} \exp[\iota(\xi x + \eta y + \gamma z)] M_i(\xi, \eta) \frac{d\xi d\eta}{\gamma}, \quad (25)$$

for

$$z > 0, \quad (26)$$

where

$$M_i(\xi, \eta) = \frac{-2\iota\omega_i}{ab} \iint_{S_p} \Phi_i^T \phi \exp[-\iota(\xi x + \eta y)] dx dy. \quad (27)$$

In Eqs. (25)–(27) the symbol $k_e = \omega_i/c$ is the acoustic wavenumber; ξ , η and γ are the components of the acoustic wavevector; ρ_e and c are the air density and the sound velocity in air, respectively; ι is the imaginary number satisfying equation $\iota^2 = -1$; and Φ_i is the i -th eigenvector (i -th column in the eigenvector matrix Φ).

To determine an estimate of the modal acoustic power, P_i , the squared modal sound pressure under freefield conditions, $p_i(x, y, z)$, can be averaged over a surface S_e , which encloses the vibrating plate. Hence, the modal acoustic power P_i can be expressed as

$$P_i = \iint_{S_e} |p_i(x, y, z)|^2 dS_e. \quad (28)$$

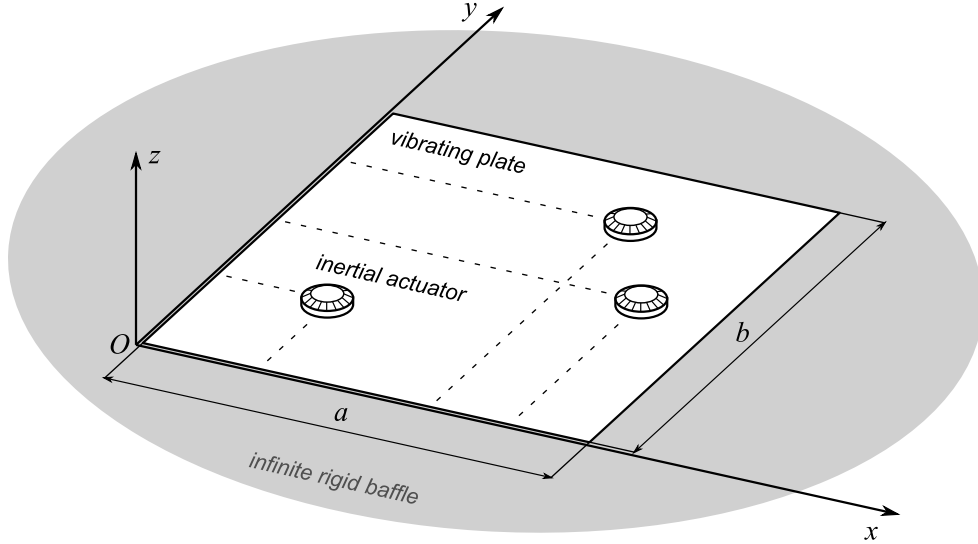


Figure 1: A schematic representation of the vibrating plate with inertial actuators, placed in an infinite rigid baffle.

In theoretical analysis the enclosing surface S_e is often defined as a hemisphere of a sufficient radius. However, to allow for the experimental verification of the model, the surface S_e will be adopted as a limited plane parallel to the plate and at a distance greater than zero. This may affect to some extent the overall estimate of the modal acoustic power, but the alteration is negligible from the point of view of actuator positioning (the absolute values of P_i may be considerably different, but the relation between the estimates of P_i obtained for different modes remain consistent, thus allowing the weakly radiating modes to be distinguished from stronger ones).

Controllability of the system

Taking advantage of the fact that the model is expressed in the state-space form, classical methods can be used to describe the controllability of the system [29, 30]. The energy-based approach has been employed, and the obtained results are later used in the optimization process for active control purposes.

The control energy required to reach the desired state \mathbf{x}_{t_1} at time $t = t_1$, assuming the optimal solution, can be expressed as

$$E_c = \int_0^{t_1} \mathbf{u}^T(t) \mathbf{u}(t) dt = (e^{A t_1} \mathbf{x}_0 - \mathbf{x}_{t_1})^T \mathbf{W}^{-1}(t_1) (e^{A t_1} \mathbf{x}_0 - \mathbf{x}_{t_1}), \quad (29)$$

where $\mathbf{W}(t_1)$ is the controllability Gramian matrix of dimensions $(2N \times 2N)$. To minimize the required control energy with respect to the locations of the actuators, a measure of the Gramian matrix should be maximized. It has been shown in the literature that instead of using $\mathbf{W}(t_1)$, a steady state controllability Gramian matrix \mathbf{W}_c can be used for stable systems when time tends to infinity [31]. This controllability Gramian matrix can be calculated by solving the Lyapunov equation, which gives

$$\mathbf{A} \mathbf{W}_c + \mathbf{W}_c \mathbf{A}^T + \mathbf{B} \mathbf{B}^T = 0. \quad (30)$$

The controllability Gramian matrix is convenient to use, because if the $(2i)$ -th value on the diagonal of the matrix, $\lambda_{c,i}$, which corresponds to the i -th eigenmode, is small, the eigenmode is difficult to control (it can be regulated only if a large control energy is available). Hence, the values $\lambda_{c,i}$ should be maximized in order to improve the susceptibility of the system to control inputs. The values $\lambda_{c,i}$ depend on the actuators arrangement. Such information can be an important criterion in the optimization of the actuator placement. Formally, controllability is a dichotomous property, but “controllable” does not indicate the level of control effort that is needed to reach the final state.

The state-space system employed in the controllability evaluation includes only vibration phenomena (the acoustic radiation weighting is not incorporated). This is because expressing the acoustic radiation as a separate term (cf. Section 4.2) provides more flexibility in the cost function design step.

Summary

The derived model of the vibroacoustic system, although based on components available in the literature, combines both vibration and acoustic radiation phenomena in a concise and coherent form, and also takes into account the loading of the plate due to the inertial actuators used for active control. The employment of the Rayleigh-Ritz method facilitates a numerical solution of

the system to be found, while the state-space representation enables analysis of the controllability of the system. All of these components provide a complete and reliable model of thin plates used as active noise barriers, which can be applied to optimize the actuator arrangement and is one of the main contributions of this paper.

3. Experimental verification of the model

In this Section, results from an experimental verification of the developed model are presented. For this purpose, an unloaded aluminium plate was used. The plate was attached to a rigid cubic frame. The remaining walls, which were constructed from sound-absorbing materials, were also attached to the frame to form a closed box. The aluminium plate was acoustically excited by a loudspeaker placed inside the box. The loudspeaker was driven by white noise bandlimited up to 1 kHz. Photographs of the laboratory setup are presented in Fig. 2.

The dimensions of the plate area that was free to vibrate (i.e. the area inside the square clamping frame) were equal to $0.420 \text{ m} \times 0.420 \text{ m}$. The plate can be described by the following parameters, which are defined in the model developed in Section 2:

$$\begin{aligned} a &= 0.420 \text{ m}, & b &= 0.420 \text{ m}, & h &= 0.001 \text{ m}, \\ E_x &= 70 \text{ GPa}, & \rho_p &= 2770 \text{ kg/m}^3, & \nu_x &= 0.3, \\ E_y &= 77 \text{ GPa}, & G &= 26.9 \text{ GPa}. \end{aligned}$$

Firstly, the accuracy of the model of the plate vibration was evaluated. The response of the plate was measured using a laser vibrometer (Polytec PDV-100). The vibrometer was mounted on

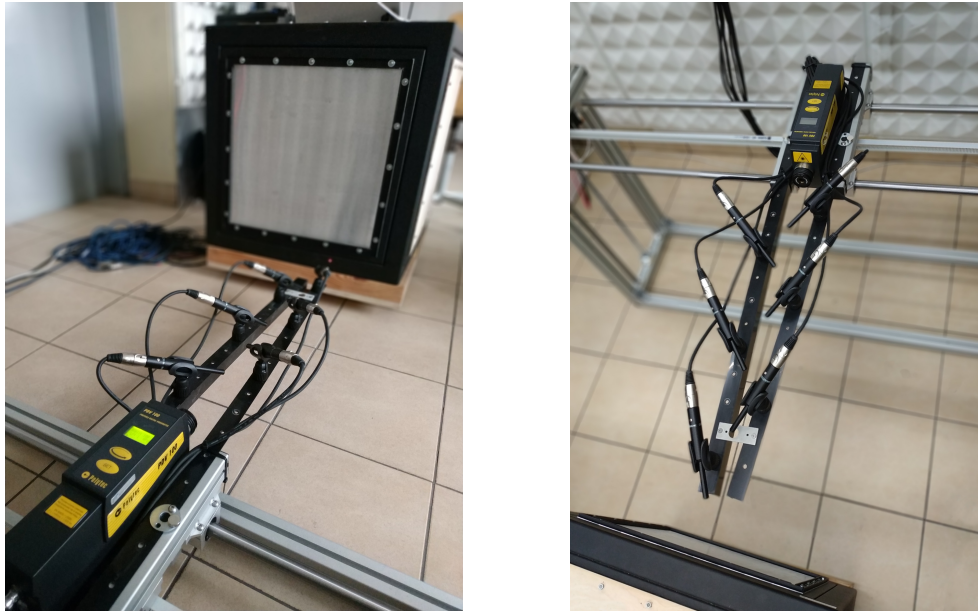


Figure 2: Photographs of the laboratory setup with an unloaded plate attached to a rigid cubic frame and excited with a loudspeaker placed inside the frame. An automatic positioning system for the laser vibrometer is also shown.

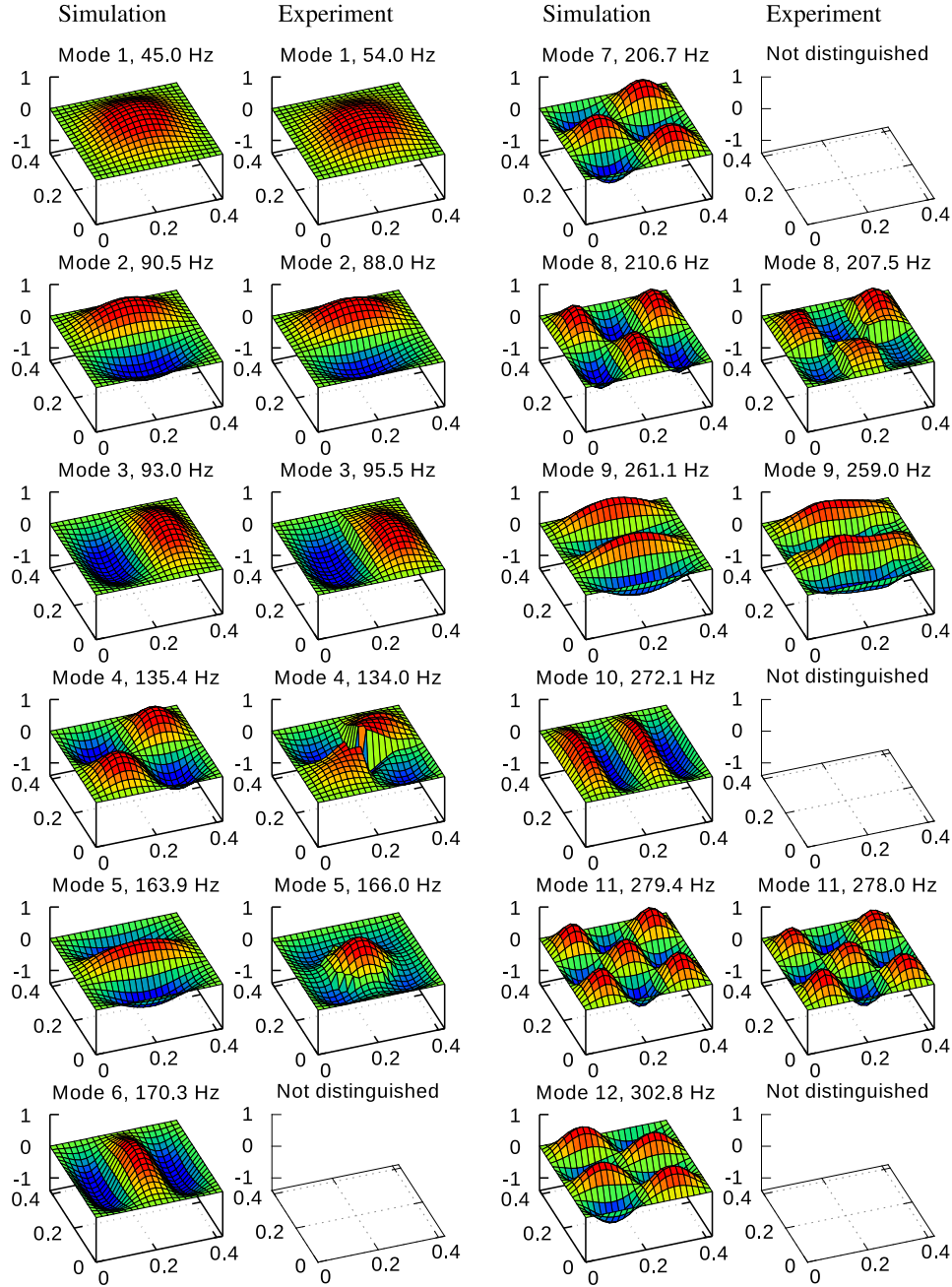


Figure 3: A comparison of the first 12 natural frequencies of rigid casing wall, and mode shapes calculated with the mathematical model and experimentally measured operational vibration shapes—1 mm thick aluminium unloaded plate. Size of the plate is in [m], and the z-axis depicts normalized amplitude.

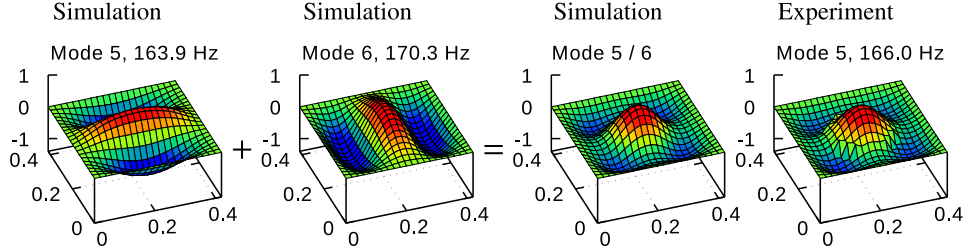


Figure 4: A comparison between the theoretically calculated vibration mode shapes 5 and 6, and their superposition with the experimentally measured operational vibration shape 5.

an automatic positioning system developed by the authors (cf. Fig. 2). Vibration measurements were taken over a uniform grid of 22×22 points (the interval between points was equal to 0.02 m).

Subsequently, the model of the acoustic radiation from the plate was also examined. For this purpose, the carriage with the laser vibrometer was complemented with an array of six measurement microphones (Beyerdynamic MM1). The microphones were arranged to measure the sound pressure just above the laser beam at distances from the plate of between 0.1 m and 0.6 m in steps of 0.1 m; this gives a total of 3120 measurement positions.

3.1. Verification of the modelling of plate vibrations

A comparison between the results from the experimental measurements and those calculated using the model is presented in Fig. 3. From these results it can be seen that the consistency between the results is very good, both in terms of the natural frequencies and mode shapes. Some of the modes could not be distinguished with the laboratory setup, which is due to two facts. Firstly, not all of the modes were equally excited with the loudspeaker, which means that weakly excited modes could not be distinguished well enough from the background noise. Secondly, if two modes have similar natural frequencies but significantly different magnitudes, then the more strongly excited mode would dominate and the weakly excited could not be observed. However, it is clear from the presented results that the majority of the first 12 vibrational modes of the plate were captured and are very consistent with the model.

It is worthwhile to provide an additional comment regarding the experimentally measured fifth operational vibration shape. This shape is in fact a superposition of the theoretically calculated modes 5 and 6. This phenomena is visualized in the Fig. 4 which shows the theoretically calculated mode shapes for modes 5 and 6 and their combination, along with the experimentally identified 5th operational vibration shape. This behaviour is typical for square plates, because pairs of natural frequencies are often very close to each other. If the magnitudes of such modes are similar, the coupled shapes can be observed, as in the case of the experimental setup considered here.

It is also noteworthy that the experimentally measured natural frequencies of related pairs of modes, e.g. mode 2 and 3, are not equal (for a square isotropic plate, these frequencies should be equal). This leads to the conclusion that even a material that could be expected to be isotropic (a common flat aluminium plate), may in fact be orthotropic to some extent, which may be due to the manufacturing process of the metal sheets. This is important because it justifies the selection of the orthotropic form of the developed model, which could otherwise be replaced by the simpler isotropic model.

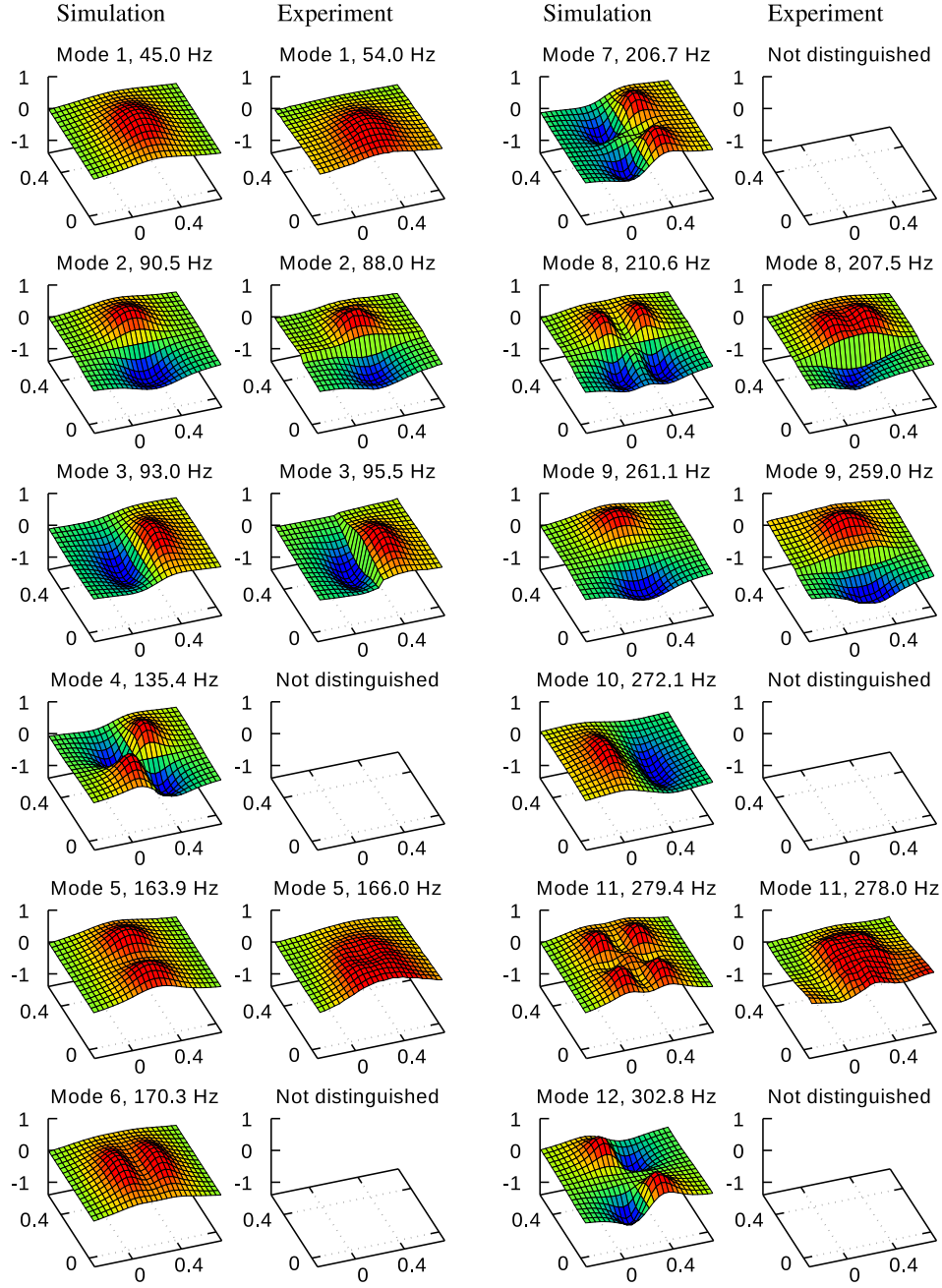


Figure 5: A comparison of initial 12 modal sound pressure distributions in the near field of the rigid casing wall, calculated with the mathematical model and experimentally measured—1 mm thick aluminium unloaded plate. Size of the measurement grid is in [m], and the z-axis depicts normalized amplitude.

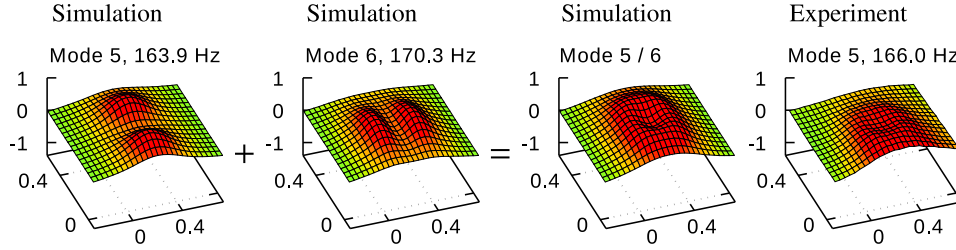


Figure 6: A comparison between the theoretically calculated modal sound pressure distributions in the near field for modes 5 and 6, and their superposition with the experimentally measured mode 5.

3.2. Verification of the modelling of the acoustic radiation from the plate

A comparison between the experimental acoustic measurements and the theoretical calculations is presented in Fig. 5. The visualized modal sound pressure distributions reflect the sound pressure measured and simulated for the first 12 natural frequencies over a measurement grid. The presented grid was 1.00 m wide and 0.64 m high, and located at a distance of 0.1 m from the plate surface, with an interval between the measurement points of 0.04 m; this gives 26×17 measurement points, which is a total of 442 points). Assuming that the origin of the coordinate system was placed at the lower left corner of the plate, then the covered area can be defined by the following coordinates: $x \in [-0.29, 0.71]$, $y \in [-0.08, 0.56]$ and $z = 0.1$.

From Fig. 5 it can be seen that there is a high level of consistency between the experimental and theoretical results. As discussed in the previous section in relation to the measurements of

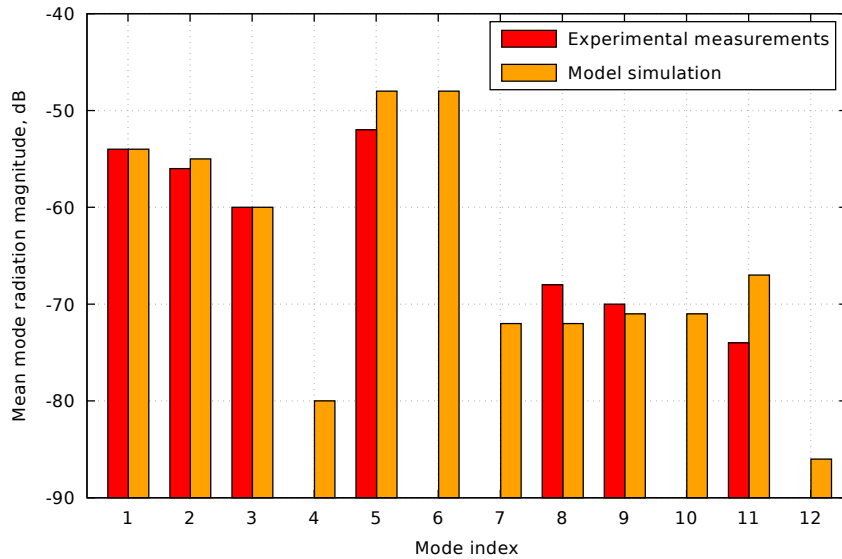


Figure 7: A comparison between the mean mode magnitudes obtained by experimental measurements and model simulations. The mean values were obtained by averaging over a plane parallel to the plate at a distance of 0.1 m.

the vibration response, if a particular mode was sufficiently excited to be accurately measured, then the measurements are consistent with the model. Once again, the fifth mode is worth an additional comment—the observed shape, as in case of the vibration response, is a result of the superposition of the theoretically calculated modes 5 and 6. This phenomena is visualized in the Fig. 6.

For the acoustic measurements, it is also worthwhile to compare the mean mode magnitudes obtained by experimental measurements with the theoretical expectations. This comparison is presented in Fig. 7. Based on the measured vibration magnitudes, the mean sound pressure magnitudes due to the individual modes obtained through the experimental measurements and the model simulations can be compared. The mean values were obtained by averaging over the described measurement grid at a distance of 0.1 m from the plate surface. It follows from the analysis of Fig. 7 that the accuracy of the theoretical prediction is very high, especially taking into account the fact that the utilized acoustic laboratory is not an anechoic chamber and the room acoustics interfere with the measurement to some extent. Hence, the conclusion can be drawn that the model has been successfully verified and that it can be used for the optimization process presented in the following Section.

4. Optimization process

In this section an optimization process is presented that aims to find the optimal placement of a number of actuators mounted to a vibrating plate for the purpose of active control. The objective of the control system is to reduce the noise radiated from the acoustic enclosure via the Active Structural Acoustic Control (ASAC) approach [32, 33]. In order to reach this goal, the control system should be able to control the vibration modes of the plate in the frequency range of interest. The ability to control the i -th mode can be described by an element on the diagonal of the controllability Gramian matrix, $\lambda_{c,i}$, as derived in Section 2. However, some of the vibrational modes are more important as they more strongly transmit or radiate noise when excited; while other modes behave in the exactly opposite manner and can be neglected, since they vibrate without strongly contributing to the radiated acoustic field. In order to reflect this behaviour, the modal acoustic power corresponding to i -th vibration mode of the plate, P_i , can be used (cf. Section 2). Taking this into account, an optimization problem defined by an appropriate cost function will be presented, which will enable an optimal solution to be found for the arrangement of the given actuators.

4.1. Optimization problem

The optimization variables defined for the considered problem are the coordinates of a pre-defined number of actuators, N_a . A flat rectangular plate is considered, hence two coordinates per i -th actuator, $x_{a,i}$ and $y_{a,i}$, are sufficient to unambiguously describe its location. Hence, the optimization algorithm is required to find a solution in an $2N_a$ -dimensional space.

Due to physical dimensions of the actuators, certain constraints have to be defined in order to maintain the practicability of the solution. Namely, margins from the plate edges and between the actuators should be maintained, with the assumption that the actuators can be attached only from one side of the plate. Inertial actuators are considered in this paper, which are most commonly manufactured with a round foot print, although the method could be extended to more complex geometries as required. The first resulting constraint ensures that the actuators are placed within the boundaries of the plate; the dimensions of the considered rectangular plate are $a \times b$, hence,

the coordinates of i -th actuator $x_{a,i} \in (\frac{1}{2}d_{a,i}, a - \frac{1}{2}d_{a,i})$ and $y_{a,i} \in (\frac{1}{2}d_{a,i}, b - \frac{1}{2}d_{a,i})$, where $d_{a,i}$ is the diameter of the i -th actuator. The second constraint ensures that actuators do not overlap; for $i \neq j$, the i -th and j -th actuators should not be closer than a distance of $\frac{1}{2}d_{a,i} + \frac{1}{2}d_{a,j}$, which is represented by the following constraint: $(x_{a,i} - x_{a,j})^2 + (y_{a,i} - y_{a,j})^2 \geq (\frac{1}{2}d_{a,i} + \frac{1}{2}d_{a,j})^2$.

4.2. Cost functions

The cost functions for the described problem can be formulated in a number of ways. In this research, six cost functions will be evaluated and analysed. Firstly, three cost functions that do not take into account the acoustic radiation, J_1 - J_3 , are formulated as follows,

$$J_1 = \min_i \lambda_{c,i}, \quad (31a)$$

$$J_2 = N_J^{-1} \left(\sum_i \lambda_{c,i} \right), \quad (31b)$$

$$J_3 = \left(\prod_i \lambda_{c,i} \right)^{N_J^{-1}}, \quad (31c)$$

for $i \in \{1, 2, \dots, N_J\}$, where N_J is the number of modes considered in the cost function. The same range of i is also considered for the other cost functions. All three cost functions J_1 - J_3 focus on maximizing the controllability of the system, however, they result in a different balance between the N_J controllability measures, $\lambda_{c,i}$, corresponding to the N_J considered modes. Cost function J_1 represents only the least controllable mode, and thus ensures that there are no uncontrollable resonances within the frequency range of interest. Cost function J_2 , which represents the mean controllability of the modes within the frequency range of interest, may increase the controllability of certain modes, even if this happens at the expense of reducing the controllability of other modes. Finally, cost function J_3 should lead to solutions that provide a trade-off between J_1 and J_2 , making sure that the smallest of the factors is maximized, whilst also benefiting to some extent an increase in the controllability of the other modes in the frequency range of interest.

Subsequently, three additional cost functions are defined, J_4 - J_6 , which are analogous to the initial three cost functions, but take into account the acoustic radiation. These cost functions are defined as

$$J_4 = \min_i \left(\frac{\lambda_{c,i}}{P_i} \right), \quad (32a)$$

$$J_5 = N_J^{-1} \left(\sum_i \frac{\lambda_{c,i}}{P_i} \right), \quad (32b)$$

$$J_6 = \left(\prod_i \frac{\lambda_{c,i}}{P_i} \right)^{N_J^{-1}}. \quad (32c)$$

In each case, the division of $\lambda_{c,i}$ by P_i forces the optimization algorithm to seek solutions with better controllability (more energy efficient) for the i -th mode, if the i -th mode acoustic radiation measure P_i is higher. That is, the cost functions are weighted to focus the effort into the controllability of the strongly radiating structural modes.

4.3. Optimization algorithm

The search space that follows from the optimization problem described in the previous subsections is very complicated and contains numerous local maxima. Therefore, an efficient algorithm must be employed in order to find a solution that satisfies the defined requirements. A Memetic Algorithm (MA) can be utilised for such a task, which is a hybrid form of a population-based approach coupled with separate individual learning [34]. The MA combines advantages of a global search, as offered by evolutionary algorithms, and local refinement procedures, which enhance convergence to the local maxima [34, 35]. Due to these complementary properties, MA are particularly suitable for solving complex multi-parameter optimization problems, such as the placement of sensors and actuators [36, 37].

5. Analysis of optimization results

In this Section, an analysis of the optimization results obtained for the arrangement of real actuators is presented. Dayton Audio DAEX32EP-4 are considered as actuators in this paper. They have a circular form factor, with a mass $m_{a,i} = 0.115$ kg and a diameter $d_{a,i} = 0.060$ m. The dimensions of the considered plate are $a = 0.420$ m and $b = 0.420$ m, hence, based on the constraints defined in Subsection 4.1 the coordinates of the i -th actuator are given as $x_{a,i} \in (0.030, 0.390)$, $y_{a,i} \in (0.030, 0.390)$ and $(x_{a,i} - x_{a,j})^2 + (y_{a,i} - y_{a,j})^2 \geq (0.060)^2$ for $i \neq j$.

The configurations for three, six and nine actuators have been optimized using the six cost functions, J_1 - J_6 , defined in the previous Section. The objective was to maximize the controllability of the plate used as an active acoustic barrier. The low frequency range was considered, hence the first $N_f = 12$ vibration modes of the plate were considered in the optimization process. The obtained results are summarized in Tab. 1.

It follows from an analysis of the results presented in Tab. 1 that the introduction of an acoustic radiation estimate into the cost function J_1 , obtaining J_4 , enables an increase in the controllability measure $\lambda_{c,i}$ of more than 5 dB for acoustically-relevant modes (where $P_i \geq 30$ dB; in Tab. 1 they are highlighted with a grey background). An increase in the controllability measure $\lambda_{c,i}$ means that the i -th mode is more excited with the same control effort (e.g. an increase of $\lambda_{c,i}$ by 5 dB means that the modal velocity of the i -th mode is by 5 dB greater with the same control effort). The price that is paid for this increase is a smaller controllability for modes that are less responsible for acoustic radiation or transmission. The minimal controllability measure $\lambda_{c,i}$ for J_1 is 50 dB, while for J_4 it is 40 dB. However, the least controllable mode for the solution obtained with J_4 has $P_i = 19$ dB, which means that its role in acoustic radiation or transmission will be minor compared to the other modes that have a P_i that is more than 15 dB higher.

It is also interesting to highlight that modifying cost function J_1 to give J_4 provides a similar increase in the controllability of the acoustically-relevant modes to that achieved by employing additional actuators, as shown by the results presented in Tab. 2. By optimizing the actuator locations using J_4 , a similar controllability can be reached as achieved when the number of actuators are doubled and optimized using J_1 . In other words, by using J_4 the number of actuators, N_a , could be reduced, e.g. from 6 to 3 per plate, whilst maintaining a similar level of controllability in terms of the acoustically-relevant modes. In practical noise control applications, this reduction in the required number of actuators offers a significant reduction in the cost and control system complexity, which is a considerable advantage.

Referring again to the results presented in Tab. 1 it can be seen that the results obtained for both J_2 and J_5 are in general inferior to the results obtained with J_1 and J_4 . The reason for this is

that if a sum is employed in the cost function (J_2 and J_5), it can be beneficial to maximize only one component of the sum and neglect the others. In the considered optimization problem, the controllability of the first mode was maximized, but the remaining modes were neglected and, as a result, these cost functions do not meet the objective.

It is interesting to note from the results presented in Tab. 1 that both J_1 and J_3 result in similar cost function values. The controllability of all considered modes has been maximized using these cost functions. However, introduction of acoustic radiation measure into cost function J_3 , which gives J_6 , provides unsatisfactory results. It turns out that it is beneficial for J_6 to have a single mode of high acoustic radiation and lower controllability, while maximizing controllability of the other less acoustically-relevant modes. This is, therefore, an unacceptable solution for the

Table 1: Results of the optimization for cost functions J_1 - J_6 with $N_a = 3$ and $N_f = 12$. The natural frequencies ω_i are given in [Hz], while values of the cost functions J_1 - J_6 , $\lambda_{c,i}$, P_i and $\lambda_{c,i}/P_i$ are given in [dB]. Resulting values of the cost functions used as the optimization index are marked with bold font. Individual modes of high acoustic radiation ($P_i \geq 30$ dB) are highlighted with a grey background. The actuators placement is also given.

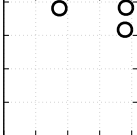
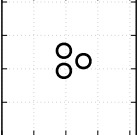
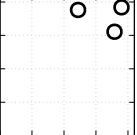
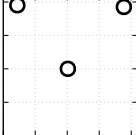
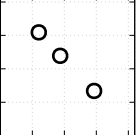
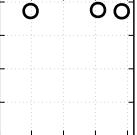
		Cost functions used in the optimization																							
		Neglecting the acoustic radiation												Taking into account the acoustic radiation											
		J1				J2				J3				J4				J5				J6			
Obtained values	J1	50				11				49				40				29				47			
	J2	55				62				56				58				61				55			
	J3	53				33				54				51				46				53			
	J4	17				-12				17				21				8				13			
	J5	33				41				32				34				43				35			
	J6	29				9				28				25				22				32			
			ω_i	$\lambda_{c,i}$	P_i	$\frac{\lambda_{c,i}}{P_i}$	ω_i	$\lambda_{c,i}$	P_i	$\frac{\lambda_{c,i}}{P_i}$	ω_i	$\lambda_{c,i}$	P_i	$\frac{\lambda_{c,i}}{P_i}$	ω_i	$\lambda_{c,i}$	P_i	$\frac{\lambda_{c,i}}{P_i}$	ω_i	$\lambda_{c,i}$	P_i	$\frac{\lambda_{c,i}}{P_i}$	ω_i	$\lambda_{c,i}$	P_i
Modes	1	43	55	28	27	20	73	21	52	41	60	28	32	29	68	24	44	26	69	23	46	44	54	28	26
	2	75	58	22	36	69	41	22	19	65	60	26	34	82	47	23	24	45	65	18	47	72	61	21	39
	3	77	59	21	38	72	36	20	16	81	60	21	39	85	43	21	22	67	63	11	52	76	59	21	38
	4	102	52	21	31	109	49	37	13	100	54	22	32	113	56	35	21	83	36	20	16	103	51	21	30
	5	119	54	22	33	133	34	24	11	113	54	20	33	116	55	34	21	117	53	34	19	110	56	22	33
	6	136	56	19	37	142	23	25	-2	129	56	23	33	132	56	35	21	129	29	22	8	130	58	20	37
	7	146	50	22	28	155	37	28	9	151	51	29	22	149	52	17	35	137	46	34	12	155	51	16	35
	8	178	50	32	19	175	22	21	1	176	49	28	21	166	40	19	21	160	33	23	10	168	48	19	29
	9	184	50	33	17	220	13	24	-12	183	51	22	29	186	48	27	21	167	43	31	12	179	48	34	13
	10	194	50	19	31	225	11	15	-5	184	51	33	17	189	47	25	22	194	33	26	8	197	47	14	33
	11	203	50	30	20	247	38	30	8	201	50	27	23	217	51	23	27	212	42	27	15	199	53	14	38
	12	212	52	22	30	301	14	22	-8	212	50	27	22	223	48	22	26	236	42	23	20	203	50	17	34
Actuators placement	i	$x_{a,i}$ (m)		$y_{a,i}$ (m)		$x_{a,i}$ (m)		$y_{a,i}$ (m)		$x_{a,i}$ (m)		$y_{a,i}$ (m)		$x_{a,i}$ (m)		$y_{a,i}$ (m)		$x_{a,i}$ (m)		$y_{a,i}$ (m)		$x_{a,i}$ (m)		$y_{a,i}$ (m)	
	1	0.379		0.317		0.194		0.254		0.380		0.384		0.377		0.385		0.187		0.239		0.097		0.373	
	2	0.382		0.383		0.255		0.223		0.358		0.311		0.044		0.390		0.120		0.309		0.308		0.376	
	3	0.174		0.381		0.194		0.194		0.244		0.376		0.202		0.200		0.293		0.134		0.382		0.372	
	An overview:				An overview:				An overview:				An overview:				An overview:				An overview:				
																									

Table 2: Results of the optimization for the cost functions J_1 and J_4 with $N_J = 12$ and N_a equal to 3, 6 or 9. The natural frequencies ω_i are given in [Hz], while values of the cost functions J_1 and J_4 , $\lambda_{c,i}$, P_i and $\lambda_{c,i}/P_i$ are given in [dB]. Resulting values of the cost functions used as the optimization index are marked with bold font. Individual modes of high acoustic radiation ($P_i \geq 30$ dB) are highlighted with a grey background. The placement of the actuators is also given.

Cost functions used in the optimization																	
	J1												J4				
	$N_a = 3$				$N_a = 6$				$N_a = 9$				$N_a = 3$				
Obtained values	J1	50				53				56				40			
	J2	55				59				63				58			
	J3	53				56				59				51			
	J4	17				19				21				21			
	J5	33				38				44				34			
	J6	29				31				37				25			
Modes		ω_i	$\lambda_{c,i}$	P_i	$\frac{\lambda_{c,i}}{P_i}$	ω_i	$\lambda_{c,i}$	P_i	$\frac{\lambda_{c,i}}{P_i}$	ω_i	$\lambda_{c,i}$	P_i	$\frac{\lambda_{c,i}}{P_i}$	ω_i	$\lambda_{c,i}$	P_i	$\frac{\lambda_{c,i}}{P_i}$
	1	43	55	28	27	32	66	25	41	22	71	22	48	29	68	24	44
	2	75	58	22	36	46	65	19	47	40	66	14	52	82	47	23	24
	3	77	59	21	38	79	56	28	29	61	60	26	34	85	43	21	22
	4	102	52	21	31	86	53	23	30	71	60	21	39	113	56	35	21
	5	119	54	22	33	104	57	24	33	82	60	14	47	116	55	34	21
	6	136	56	19	37	114	56	28	28	90	57	18	38	132	56	35	21
	7	146	50	22	28	124	55	31	25	104	58	17	41	149	52	17	35
	8	178	50	32	19	132	55	24	31	112	56	31	25	166	40	19	21
	9	184	50	33	17	144	53	15	38	121	56	27	29	186	48	27	21
	10	194	50	19	31	152	53	34	19	127	56	29	27	189	47	25	22
	11	203	50	30	20	174	53	29	24	141	56	20	37	217	51	23	27
	12	212	52	22	30	186	53	25	28	147	56	36	21	223	48	22	26
Actuators placement	i	$x_{a,i}$ (m)	$y_{a,i}$ (m)	$x_{a,i}$ (m)	$y_{a,i}$ (m)	$x_{a,i}$ (m)	$y_{a,i}$ (m)	$x_{a,i}$ (m)	$y_{a,i}$ (m)	$x_{a,i}$ (m)	$y_{a,i}$ (m)	$x_{a,i}$ (m)	$y_{a,i}$ (m)				
	1	0.379	0.317	0.380	0.272	0.214	0.118	0.377	0.385								
	2	0.382	0.383	0.037	0.385	0.249	0.050	0.044	0.390								
	3	0.174	0.381	0.313	0.312	0.381	0.369	0.202	0.200								
	4			0.035	0.176	0.063	0.256										
	5			0.385	0.032	0.369	0.033										
	6			0.123	0.164	0.135	0.248										
	7					0.380	0.301										
	8					0.186	0.180										
	9					0.205	0.382										
An overview:		An overview:		An overview:		An overview:											

considered application.

Acoustic and structural vibration responses of the plate, obtained for the different optimization indices J_1 - J_6 , are presented in Fig. 8. These responses are calculated for the solutions summarized in Tab. 1, hence in all cases the number of actuators $N_a = 3$. Both responses, driven

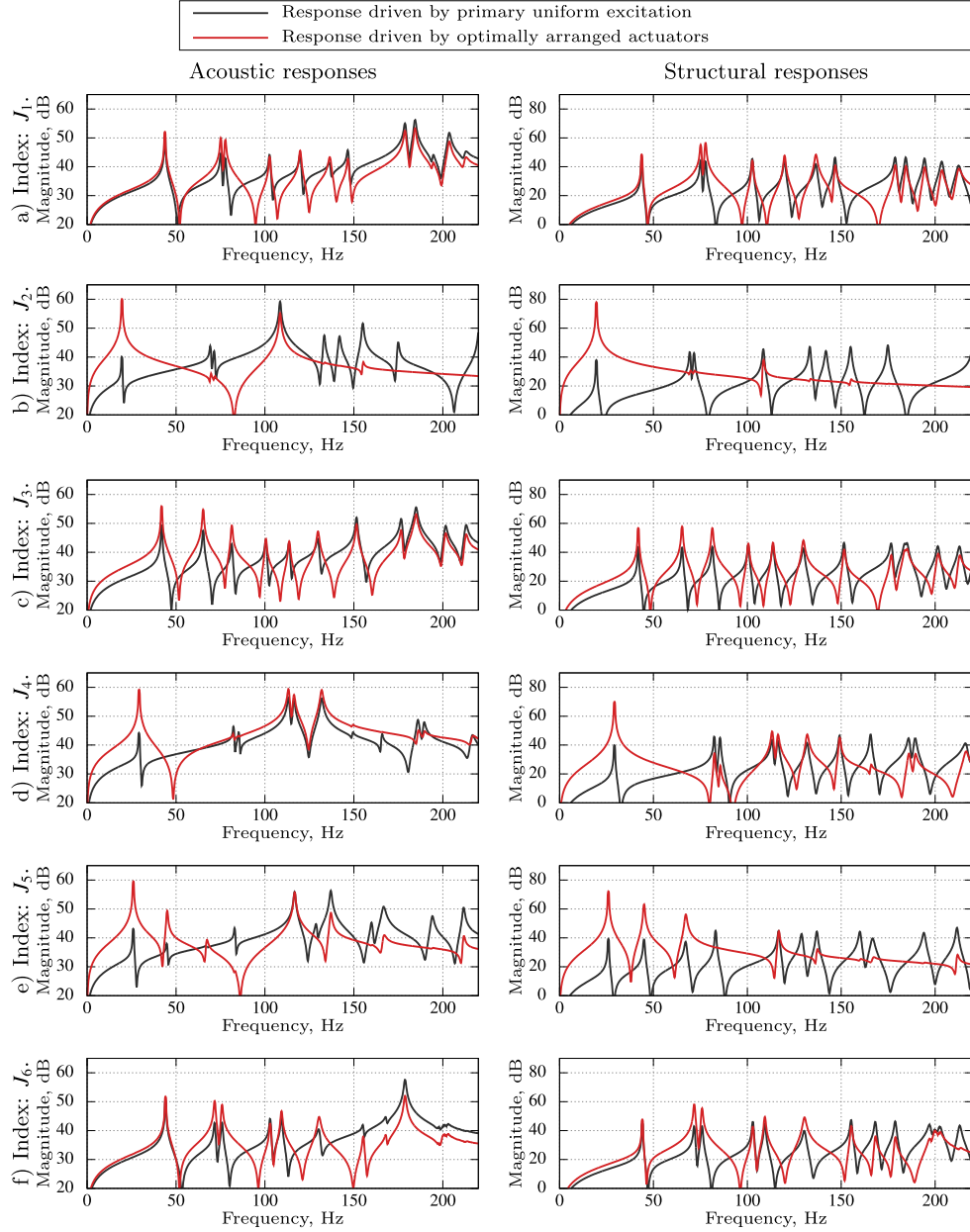


Figure 8: Acoustic and structural vibration responses of the plate, obtained for different optimization indices J_1 - J_6 as summarized in Tab. 1. Responses are shown for both the primary uniform excitation and when excited using the optimally arranged actuators.

with the primary uniform excitation and by the optimally arranged actuators, are presented. The responses of the plate due to primary uniform excitation are obtained by applying an equal excitation to all structural modes, instead of simulating an external acoustic excitation. These responses correspond to the result of a uniform wide-band external excitation that can be produced by many types of common noise sources. The responses due to excitation by the optimally arranged actuators are obtained by simulating actuator action as forces acting at the optimized actuator locations $(x_{a,i}, y_{a,i})$. A wideband signal again was used as the input to the actuators. The magnitude of the input signals to the actuators was arbitrarily chosen and was the same in all evaluated cases and for all actuators. The larger the response due to the actuators (shown by the red line) compared to the response when driven by the primary uniform excitation (shown by the black line), the easier it will be for the control system to reduce the noise transmission or radiation in the considered frequency range.

It follows from analysis of Fig. 8 that in the case of the structural responses obtained for J_1 and J_3 , the responses due to optimally arranged actuators nearly match for all considered peaks in the responses due to primary uniform excitation. However, in the case of the acoustic responses obtained for J_1 and J_3 , the highest peaks in the responses due to primary uniform excitation are higher than the corresponding responses due to the actuators, while the response due to the optimally arranged actuators obtained for J_4 dominates the highest peaks in the acoustic response of the plate due to primary uniform excitation. Still, an enhanced performance in acoustic response obtained for J_4 is traded for a weaker structural response for the modes that are less responsible for acoustic radiation or transmission. These remarks are consistent with the previous conclusions drawn from the analysis of Tab. 1.

6. Conclusions

Active noise control methods are gaining growing attention as a practical method for controlling noise in the increasingly noise-polluted world. This paper develops a new acoustic radiation-based method to optimize the arrangement of actuators for active noise barriers. A model of acoustic radiation was introduced into the optimization process and new cost functions were formulated in order to focus on modes that are truly relevant to the noise transmission and radiation. This optimization process constitutes the main novelty of the presented research. The study involved mathematical modelling, laboratory experiments and numerical simulations in order to evaluate the proposed optimization method.

The employed model was validated experimentally and employed in the optimization of the actuators for a real laboratory setup. It follows from an analysis that introduction of the acoustic radiation measure into the cost function in the form of J_4 offers best performance and enables an increase in the controllability measure of more than 5 dB for acoustically-relevant modes. The increase in controllability for these modes is comparable to that achieved by employing additional actuators (at least doubling the number of actuators for the considered system). From a different point of view, this method could also be used to rearrange the actuators in order to try to reduce their number, while maintaining the same level of controllability. Such reduction in practical noise control applications entails a significant reduction in the cost and the control system complexity.

These advantages are traded for a reduction in the controllability of the modes that are less responsible for acoustic radiation or transmission. However, such modes have been shown to have a modal acoustic power that is at least 15 dB lower than that due to the dominant modes, which means that their contribution to the noise transmission and radiation is negligible.

Acknowledgment

The research reported in this paper has been supported by the National Science Centre, Poland, decision no. DEC-2017/25/B/ST7/02236.

References

- [1] S. Cinquemani, M. Bassetti, and F. Resta. Design and testing of a mechatronic device to actively self suppress vibration in structures. *International Journal of Acoustics & Vibration*, 23(2), 2018.
- [2] Y. Pu, H. Zhou, and Z. Meng. Multi-channel adaptive active vibration control of piezoelectric smart plate with online secondary path modelling using pzt patches. *Mechanical Systems and Signal Processing*, 120:166–179, 2019.
- [3] X. Xie, M. Ren, D. Yang, and Z. Zhang. Simulation and experiment on tonal vibration transmission control with a multi-channel global control method. *Mechanical Systems and Signal Processing*, 138:106563, 2020.
- [4] J. Gripp and D. Rade. Vibration and noise control using shunted piezoelectric transducers: A review. *Mechanical Systems and Signal Processing*, 112:359–383, 2018.
- [5] B. Lam, S. Elliott, J. Cheer, and W.-S. Gan. Physical limits on the performance of active noise control through open windows. *Applied Acoustics*, 137:9–17, 2018.
- [6] S. J. Elliott, J. Cheer, L. Bhan, C. Shi, and W.-S. Gan. A wavenumber approach to analysing the active control of plane waves with arrays of secondary sources. *Journal of Sound and Vibration*, 419:405–419, 2018.
- [7] S. Wang, J. Tao, X. Qiu, and J. Pan. A boundary error sensing arrangement for virtual sound barriers to reduce noise radiation through openings. *The Journal of the Acoustical Society of America*, 145(6):3695–3702, 2019.
- [8] N. Kournoutos and J. Cheer. A system for controlling the directivity of sound radiated from a structure. *The Journal of the Acoustical Society of America*, 147(1):231–241, 2020.
- [9] W. Liu, Z. Hou, and M. A. Demetriou. A computational scheme for the optimal sensor/actuator placement of flexible structures using spatial H_2 measures. *Mechanical systems and signal processing*, 20(4):881–895, 2006.
- [10] S. Chemishkian et al. H-optimal mapping of actuators and sensors in flexible structures. In *Proceedings of the 1998 37th IEEE Conference on Decision and Control (CDC)*, pages 821–826, 1998.
- [11] K. R. Kumar and S. Narayanan. The optimal location of piezoelectric actuators and sensors for vibration control of plates. *Smart Materials and Structures*, 16(6):2680, 2007.
- [12] D. Chhabra, G. Bhushan, and P. Chandna. Optimal placement of piezoelectric actuators on plate structures for active vibration control via modified control matrix and singular value decomposition approach using modified heuristic genetic algorithm. *Mechanics of advanced materials and structures*, 23(3):272–280, 2016.
- [13] S. Leleu, H. Abou-Kandil, and Y. Bonnassieux. Piezoelectric actuators and sensors location for active control of flexible structures. In *Proceedings of the 17th IEEE Instrumentation and Measurement Technology Conference*, volume 2, pages 818–823. IEEE, 2000.
- [14] J. Hale and A. Daraji. Optimal placement of sensors and actuators for active vibration reduction of a flexible structure using a genetic algorithm based on modified H_∞ . *Journal of Physics: Conference Series*, 382(1):012036, 2012.
- [15] X. Liu, G. Cai, F. Peng, and H. Zhang. Piezoelectric actuator placement optimization and active vibration control of a membrane structure. *Acta Mechanica Solida Sinica*, 31(1):66–79, 2018.
- [16] M. Misol, S. Algermissen, M. Rose, and H. P. Monner. Aircraft lining panels with low-cost hardware for active noise reduction. In *2018 Joint Conference-Acoustics*, pages 1–6. IEEE, 2018.
- [17] L. Morzyński and G. Szczepański. Double panel structure for active control of noise transmission. *Archives of Acoustics*, 43(4):689–696, 2018.
- [18] S. Wrona and M. Pawelczyk. Active reduction of device narrowband noise by controlling vibration of its casing based on structural sensors. In *Proceedings of 22nd International Congress on Sound and Vibration*, Florence, Italy, 12-16 July, 2015.
- [19] A. Chrapowska, S. Wrona, J. Rzepecki, K. Mazur, and M. Pawelczyk. Active structural acoustic control of an active casing placed in a corner. *Applied Sciences*, 9(6):1059, 2019.
- [20] J. Milton, J. Cheer, and S. Daley. Active structural acoustic control using an experimentally identified radiation resistance matrix. *The Journal of the Acoustical Society of America*, 147(3):1459–1468, 2020.
- [21] S. S. Rao. *Vibration of continuous systems*, volume 464. Wiley Online Library, 2007.
- [22] D. Young. Vibration of rectangular plates by the ritz method. *Journal of Applied Mechanics-Transactions of the ASME*, 17(4):448–453, 1950.
- [23] K. Kim, B.-H. Kim, T.-M. Choi, and D.-S. Cho. Free vibration analysis of rectangular plate with arbitrary edge constraints using characteristic orthogonal polynomials in assumed mode method. *International Journal of Naval Architecture and Ocean Engineering*, 4(3):267–280, 2012.

- [24] S. S. Rao. *Mechanical Vibrations*. Prentice Hall, 2011.
- [25] R. R. Craig and A. J. Kurdila. *Fundamentals of structural dynamics*. John Wiley & Sons, 2006.
- [26] A. N. Norris and D. M. Photiadis. Thermoelastic relaxation in elastic structures, with applications to thin plates. *The Quarterly Journal of Mechanics and Applied Mathematics*, 58(1):143–163, 2005.
- [27] W. Rdzanek. *Structural vibroacoustics of surface elements [in Polish: Wibroakustyka strukturalna elementów powierzchniowych]*. Rzeszów University of Technology Publishing House, 2011.
- [28] E. Skudrzyk. *The foundations of acoustics: basic mathematics and basic acoustics*. Springer Science & Business Media, 2012.
- [29] J. Klamka. Controllability of dynamical systems. a survey. *Bulletin of the Polish Academy of Sciences: Technical Sciences*, 61(2):335–342, 2013.
- [30] J. Wyrwał. Simplified conditions of initial observability for infinite-dimensional second-order damped dynamical systems. *Journal of Mathematical Analysis and Applications*, 478(1):33–57, 2019.
- [31] B. D. Anderson and J. B. Moore. *Optimal control: linear quadratic methods*. Courier Corporation, 2007.
- [32] K. Mazur, S. Wrona, and M. Pawelczyk. Design and implementation of multichannel global active structural acoustic control for a device casing. *Mechanical Systems and Signal Processing*, 98C:877–889, 2018.
- [33] K. Mazur, S. Wrona, and M. Pawelczyk. Active noise control for a washing machine. *Applied Acoustics*, 146:89–95, 2019.
- [34] F. Neri, C. Cotta, and P. Moscato. *Handbook of memetic algorithms*, volume 379. Springer, 2012.
- [35] J. Nalepa and M. Kawulok. Adaptive memetic algorithm enhanced with data geometry analysis to select training data for svms. *Neurocomputing*, 185:113–132, 2016.
- [36] S. Wrona, M. de Diego, and M. Pawelczyk. Shaping zones of quiet in a large enclosure generated by an active noise control system. *Control Engineering Practice*, 80:1–16, 2018.
- [37] S. Wrona and M. Pawelczyk. Shaping frequency response of a vibrating plate for passive and active control applications by simultaneous optimization of arrangement of additional masses and ribs. Part II: Optimization. *Mechanical Systems and Signal Processing*, 70-71:699–713, 2016.